AUBE '01

12TH INTERNATIONAL CONFERENCE ON AUTOMATIC FIRE DETECTION

March 25 - 28, 2001
National Institute Of Standards and Technology
Gaithersburg, Maryland U.S.A.

PROCEEDINGS

Editors: Kellie Beall, William Grosshandler and Heinz Luck

NIST
National Institute of Standards and Technology
Technology Administration, U.S. Department of Commerce

B. Farouk, G. W. Mulholland*, K. B. McGrattan* and T. G. Cleary*

Department of Mechanical Engineering and Mechanics, Drexel University
Philadelphia, PA
*Building and Fire Research Laboratory, National Institute of Standards and Technology, Gaithersburg, MD

Simulation of Smoke Transport and Coagulation for a Standard Test Fire

Abstract

Large eddy simulations of a standard test fire (EN 54-9, TF4) were carried out. The development of the large-scale air movements and temperature fields generated by the enclosure fires are calculated. In addition, the smoke transport and time evolution of the size distribution of smoke aerosol due to coagulation are also predicted. The mass and number densities of smoke particles are computed at a detector location, as specified in the standard test fire procedure. Recent measurements of the number and mass densities of smoke using electrical aerosol spectrometry compared favorably with the model predictions.

Introduction

Smoke detector response is sensitive to both the concentration of smoke within the sensing volume and the size distribution of the aerosol in a fire scenario. The object of the simulation is to compute the local smoke characteristics given the burning rate of the fire, the yield of smoke and its initial size distribution, and the geometric properties of the enclosure. Once the smoke characteristics are known at the detector location the response of the smoke detector can be computed.

Generally the ionization detectors are found to be more sensitive to the *number density* of the smoke. As a class, smoke detectors using the ionization principle provide somewhat faster response to high energy (open flaming) fires, since these fires produce larger numbers of the smaller smoke particles. On the other hand, photoelectric smoke

detectors respond to the volume *(mass) density* of the smoke particles rather than the number density.

Prediction of smoke transport and coagulation has been attempted in the past [1, 2] where the evolution of size distribution of smoke aerosol under the influence of coagulation as well as the large scale fluid motion and temperature fields were studied. Specifically, Lagrangian particles or 'thermal elements' were used to model the burning of fuel in the fire plume. Each thermal element (blob) represents a given mass of smoke (containing many smoke particles), which is proportional to the instantaneous heat release rate. The transport of the thermal elements is also used to model smoke movement (without smoke coagulation) in a Lagrangian sense. The evolution of the size distribution in space was calculated deterministically from the solution to the Smoluchowski equation.

A promising methodology for the prediction of large-scale gas movement, temperature field and smoke movement in fire plumes and enclosure fires has been recently introduced [3]. The model and computational methodology have reproduced mean temperature and buoyant velocity correlations for large fire plumes [4]. In this paper, we present numerical results for the velocity and temperature fields induced by a standard test fire (EN 54 part 9) [5] by applying the above model, which incorporates large eddy simulation techniques. The simulations reported here are for the test fire TF4 (open plastic fire) [5]. The smoke particles are again represented by a large number of the thermal elements - continuously introduced at the burning surface, while the fuel is being consumed. Based on prescribed rates of smoke yield (Y kg/kg of fuel consumed), the smoke transport within the enclosure is reported. While the ionization detectors are found to be more sensitive to the local number density of the smoke, the photoelectric detectors are more sensitive to the mass density. Hence it is necessary to determine both the mass and the number densities of the aerosol reaching a detector. A smoke coagulation sub-model based on the Smoluchowski equation [6] is incorporated to track the mean number density of smoke particles in each blob with time. The mean size of the smoke particles in each thermal element increases with time due to coagulation. The smoke mass and number densities at a specified detector location are computed directly

from the number of thermal elements and the corresponding number densities of smoke particles in each thermal element (blob), present at the detector location. The time evolution of the mass and number densities of smoke at the detector location are compared with the recent measurements reported by Mirme et al. [7]. The model predictions for smoke coagulation compare favorably with the reported measurements.

Problem description

The test fire TF4 in EN 54-9 [4] is an open plastic fire, which is allowed to burn freely with no restriction of air supply in an enclosure. The overall enclosure dimensions and the detector location are specified in the test procedure. For the present simulations, a 9.5 m x 6.3 m x 4.0 enclosure was considered (see Figure 1 below). A small vent is considered at a bottom corner of the enclosure to allow for constant pressure condition during the combustion process. The fire source is located at the center of the enclosure (0.5 m x 0.5 m) on a 0.25 m high pedestal. The walls, floor and ceiling are considered to be thermally insulated. The rate of heat release $\dot{q}(t)$ for the TF4 fire is estimated from the measurements reported by Ahonen and Sysio [8].

Model description

A fire plume is a three-dimensional transient buoyant flow that can be modeled by the motion of a thermally expandable ideal gas [8]. The Navier-Stokes equations are solved for such a fluid driven by a prescribed heat source Following Rehm and Baum [9] the pressure is decomposed into three components, a background (average) pressure, a hydrostatic contribution, and a perturbation to the hydrostatic pressure. High-frequency acoustic oscillations are eliminated while large temperature and density variations typically found in fires are retained. The resulting equations are thus referred to as weakly compressible and are valid for low Mach number flows. Constant pressure specific heat of the gas is considered in the formulation. An elliptic partial differential equation for pressure perturbation is formulated by taking the divergence of the momentum equation. Further details of the mathematical formulation can be obtained in [3].

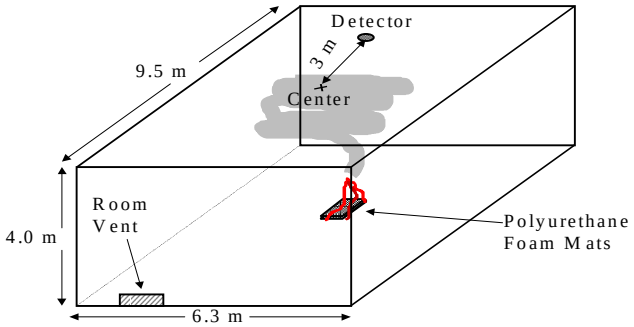

Figure 1. Schematic of the test fire laboratory

Large eddy simulation technique

The application of the large eddy simulation (LES) techniques to fire is aimed at extracting greater temporal and spatial fidelity from simulations of fire performed on the more finely meshed grids allowed by modern fast computers. The small-scale eddy motion is modeled via a sub-grid description. One such representation is the Smagorinsky model [10]. There have been numerous refinements of the original Smagorinsky model but it is difficult to assess the improvements offered by the newer schemes. In this study, we have used the Smagorinsky model, which produces satisfactory results for most large-scale applications where boundary layers are not important [3].

Combustion model

A sub-grid thermal element model (TEM) is formulated to represent the fire. A large number of Lagrangian elements (blobs) are introduced into the plume, releasing heat as they are convected by the thermally induced motion [3]. The combustion and hydrodynamics are coupled here since the fluid motion determines where the heat is released, while the heat release determines the motion. The overall heat release rate $\dot{q}(t)$ from the fire is discretized as thermal elements that represent pyrolized fuel. At a specified surface, such as the fuel bed, thermal elements are ejected at a rate of $\dot{n}''$ blobs per unit time per unit area. The heat release rate of a single thermal element 'j' is given by

$$\dot{q}_{p,j} = \frac{\dot{q}''(t_0)}{\dot{n}''}\frac{1}{t_b} \qquad (1)$$

where $\dot{q}''(t_0)$ is the instantaneous heat release rate per unit area of the fuel bed and t_b is the burnout time ($t - t_0 < t_b$) of the thermal element and t_0 is the time the element is ejected from the burning surface. The burnout time is obtained from the plume correlations of Baum and McCaffrey [4].

Smoke transport model

A specified percentage of the fuel consumed (smoke yield, Y kg/kg of fuel) is assumed to be converted to smoke particulate. The smoke transport is simulated by tracking the motion of the thermal elements. The smoke mass in any thermal element (blob) introduced at time t_0 is given by

$$m_s = \frac{\dot{q}''(t_0)\,Y}{\Delta H_c\ \dot{n}''} \qquad (2)$$

where $\dot{q}''(t_0)$ is the instantaneous heat release rate, Y is the smoke yield and ΔHc is the heat of combustion of the fuel. Again, $\dot{n}''$ is the number of thermal elements injected per unit time per unit area of the burning surface. In the present model, the total smoke mass in each blob remains constant as it is convected by the buoyant plume. At any instant, the smoke mass density at the detector location can be determined if the total number of smoke blobs in the detector volume is known. The smoke mass density is the summation of smoke masses of the individual thermal elements in a grid cell of volume $\delta x \delta y \delta z$.

$$C_m(t) = \frac{\sum m_{s,j}}{\delta x\, \delta y\, \delta z} \qquad (3)$$

Smoke coagulation model

The most important physical mechanism acting to change the smoke aerosol sized distribution once it leaves the flame zone of a fire is coagulation. The particles present at high concentration levels collide as a result of Brownian motion and stick together. The time evolution of coagulating particles for a uniform system is described by the Smoluchowski equation

$$\frac{\partial n(v,t)}{\partial t} = \int \Gamma(v-v',v')n(v-v',t)n(v',t)dv' - 2n(v,t)\int \Gamma(v,v')n(v',t)dv' \qquad (4)$$

where $n(v,t)dv$ is the number concentration in the particle volume size range v to $v + dv$ and $\Gamma(v, v')$ is the coagulation frequency. In this analysis, we assume that $\Gamma(v, v')$ is a

constant. The total number concentration, N(t) and the volume concentration V(t) are obtained as the first two moments of the size distribution. Integrating equation (3) with respect to volume leads to the following differential equation:

$$\frac{dN}{dt} = -\Gamma N^2 \qquad (5)$$

Smaller particles collide and stick decreasing the number concentration, but the volume concentration is unchanged. For the present calculations, the time evolution of the number density of smoke particles n_s (t) in a given thermal element is modeled as [5]

$$n_s(t) = \frac{n_s^o}{(1+\Gamma N^o t)} \qquad (6)$$

where n_s^0 is initial number of smoke particles in a thermal element at the time of its injection, Γ is the coagulation frequency and N^o is the initial number concentration of smoke particles (number of particles/volume) in the flame zone. For the present calculations, the value of G ($G = \Gamma N^o$) is estimated from measurements reported in literature. The initial number of smoke particles n_s^0 in a thermal element (injected at time t_0) is calculated from

$$n_s^o = \frac{\dot{q}(t_0)\, Y}{\Delta H_c\, \dot{n}''(\frac{1}{6}\pi\, D_p^3\, \rho_s)} \qquad (7)$$

where D_p is the initial smoke particle diameter (10^{-7} m)and ρ_s is the soot density (1.8 x 10^3 kg/m^3). The smoke number density is the summation of smoke masses of the individual thermal elements in a grid cell of volume $\delta x \delta y \delta z$:

$$C_N(t) = \frac{\sum n_{s,j}}{\delta x\, \delta y\, \delta z} \qquad (8)$$

where $n_{s,j}$ is defined in equation (12) above for the j-th particle.

Results and discussion

We present the results for a hypothetical fire with a 'fixed heat release rate' first. The computational domain is a parallelepiped region with a rectangular base (9.5 m x 6.3 m) and a height of 4.0 m. The origin of the Cartesian coordinate system is at the right bottom corner. A uniform mesh (64 x 32 x 32) was used for the simulations. This gives a cell size with dimensions 0.15 m x 0.20 m x 0.12 m. All simulations were

carried out for a period of 300 s. For all calculations presented, only 65% of the energy from combustion is considered to be the convective heat release. The rest of the energy, converted to radiation, did not play any role in the simulations as none of the surfaces were specified in the model as thermally active. The heat of combustion of the fuel (ΔHc) was taken as 20,000 kJ/kg. . A smoke yield value of Y = 0.05 kg/kg of fuel consumed) was used for the present simulations. Figure 2 shows the time-dependent convective heat release rate for the simulation with 'a fixed heat release rate'.

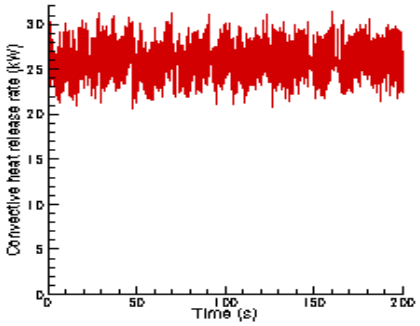

Figure 2. Convective heat release rate for the 'fixed heat release rate' case.

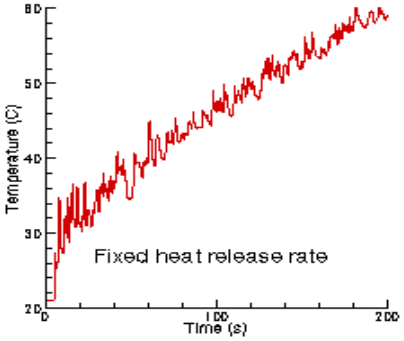

Figure 3. Predicted temperature profile at the detector location

According to EN54 – 9 specifications, the detectors and measuring instruments are to be located along a 3 m radius from the center of the fire source. A detector location was chosen near the ceiling (z = 3.9 m) at x = 2.25 m, y = 3.15 m (see Figure 1). For the present mesh, one computational cell was found to be large enough to represent a detector. The temperature rise at the detector location is shown in Figure 3 as a function of time. The temperature at the detector location continues to increase as the heat release rate is held fixed in the simulations. A large number of thermal elements were introduced into the flow field to properly characterize the smoke transport and coagulation. Five thermal elements were introduced per each cell covering the burning area per time step (ΔT = 0.05 s). All thermal elements introduced were tracked for the entire period of the calculations (200 s) unless they leave the enclosure by the small vent (see Figure 1).

The predicted smoke number density variation (averaging time = 3 s) at the detector location for the 'fixed heat release rate' case is shown in Figure 5. Coagulation effects

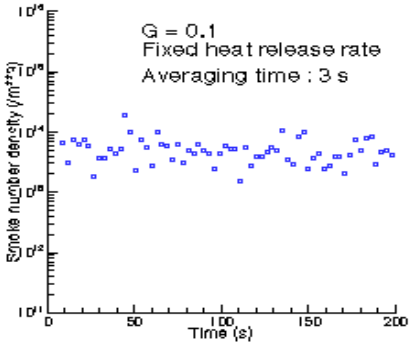

Figure 5. Predicted smoke number density $C_m(t)$at the detector location for the 'fixed heat release rate' case

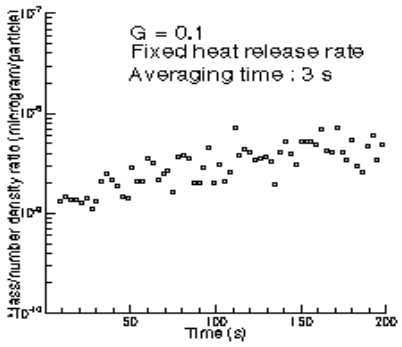

Figure 6. Ratio of smoke mass/number densities $C_m(t)/C_N(t)$at the detector location for the 'fixed heat release' case

were considered by setting G = 0.1 ¯s. The time-averaged evolution of the ratio of the smoke mass/number densities at the detector location is shown in Figure 6. The ratio increases with time as a result of the coagulation process. The greater the age of a smoke blob the larger the particle size because the smoke particle mass within the blob is constant but the number of smoke particles is decreasing in accordance with equation (6). The simulations of the test fire (TF4) are presented next. The EN54 –9 specifications suggest a fuel source of soft polyurethane foam mats (0.5 m x 0.5 m). The heat release rate for the fuel source is obtained from the measurements of Ahonen and Sysio [7]. The heat of combustion of the fuel (ΔHc) was taken as 20,000 kJ/kg and the smoke yield value was Y = 0.05 kg/kg. Figure 7 shows the time-dependent convective heat release rate for the simulations of test fire TF4.

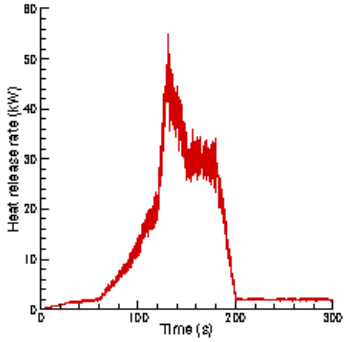

Figure 7. Convective heat release rate for the TF4 fire

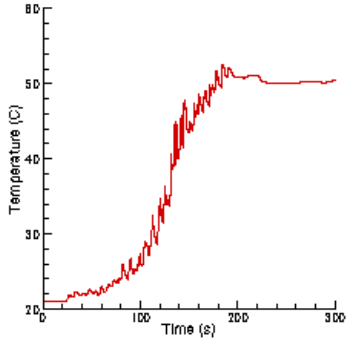

Figure 8. Predicted temperature profile at the detector location for the TF4 fire

The TF4 fire simulations were carried out for a period of 300 s. The large eddy simulations capture the evolution of the characteristic structure of the fire-plume and the associated buoyant flow field. The temperature rise at the detector location is shown in Figure 8 as a function of time. The temperature (non-averaged) at the detector location remains unchanged for the first 20 s, then increases rapidly. After the fuel source is fully consumed, the temperature is found to decrease gradually.

The predicted time variation of the smoke mass density (averaging time: 3 s) at the detector location is shown in Figure 9 for the TF4 fire. The smoke mass density increases continuously for the about 120 s (see Figure 7 for the corresponding rise in heat release rate) then levels off as the strength of the fire decreases. The recirculating flow generated in the test section maintains the level of smoke mass density at the detector location. When the calculations are carried out with no coagulation model (G = 0 ¯s), the predicted evolution of smoke mass and number densities are similar and the ratio of mass/number densities at the detector location is invariant.

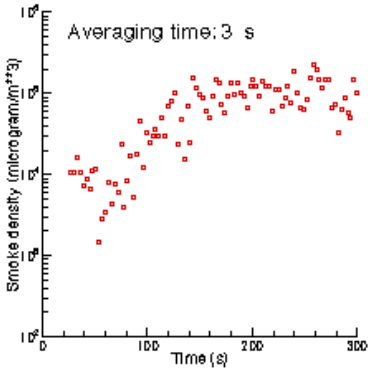

Figure 9. Time-averaged (3 s intervals) prediction of the smoke density $C_m(t)$ at the detector location for the TF4 fire

Recent measurements of the TF4 fire smoke characteristics are reported in Mirme et al. [7]. An electrical aerosol spectrometer (EAS) was used to measure the smoke aerosol characteristics including number and mass densities. The EAS is able to measure the extremely fast changing aerosol in a broad particle size range. The measured time variation of the smoke number density (top curve) and the smoke mass density (bottom curve) are shown in Figure 10.

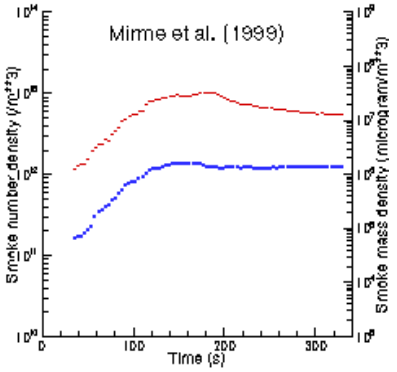

Figure 10. Measured time variation of the number and mass concentrations plastic fire (TF4).

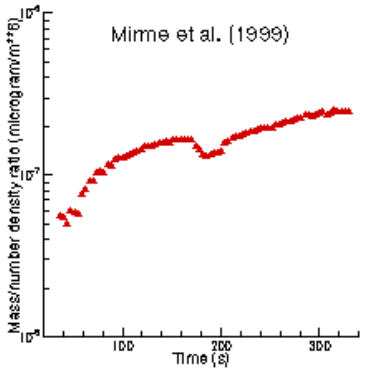

Figure 11. Measured time variation of the ratio $C_m(t)$ /$C_N(t)$ for the plastic the fire (TF4).

The ratios of the measured smoke/mass number densities are shown in Figure 11. Both the mass and number densities detected tend to increase as the fire grows with the growth rate of mass density higher than the growth rate of the number density.. While the growth rate of the mass density levels off, the number density keeps decreasing as the aerosol ages.

The model predictions for smoke coagulation for the TF4 fire (for different values of the coagulation frequency G ¯s are now presented and qualitative comparisons with the measurements (shown in Figures 10 and 11) are made. Figure 12 below shows the predicted time-averaged (averaging time: 3 s) smoke number density for the TF4 fire at the detector location with G = 0.1 ¯s. As the fire gains strength, the number density predicted increases, then starts decreasing as the coagulation effects become apparent. The trend observed in the measurements (Figure 10) is similar to that shown in the predictions in Figure 12. However, differences exist quantitatively between the measurements and the predictions. While the peak value of the measured smoke number density is about 10^{13} /m^3, the predicted peak value of the smoke number density is about 10^{14} /m^3. Also the coagulation rate predicted with G = 0.1 –s appears to be somewhat faster than the rate observed in the measurements (Figure 10, top curve).

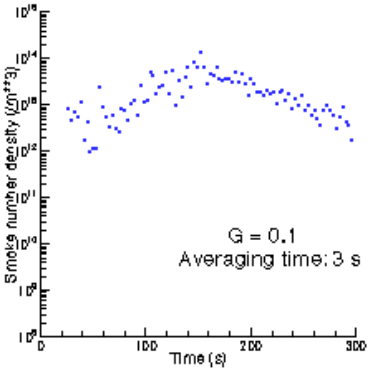

Figure 12. Time-averaged (3 s intervals) predictions of the smoke number density $C_N(t)$ at the detector location (G = 0.1 ¯s) for the TF4 fire

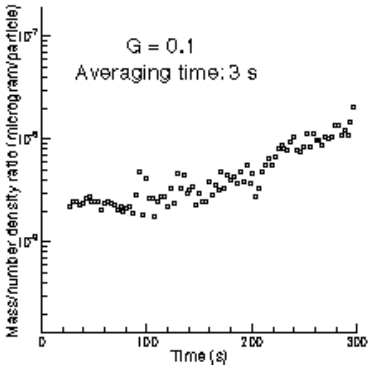

Figure 13. Time-averaged (3 s intervals) prediction of the ratio $C_m(t)$ /$C_N(t)$ at the detector location for the TF4 fire

The predicted evolution of the ratio of mass/density number densities is shown in Figure 13 with G = 0.1 ¯s. The measured ratio (as shown in Figure 11) increases as the fire develops which signifies onset of coagulation effects, though the steeper rise for times less than 80 s may result from a change in the particle size distribution during the early stages of burning. In the predictions, the $C_m(t)$ /$C_N(t)$ ratio remains somewhat invariant for the first 100 s and then starts increasing. The increase in the ratio is a result of older smoke blobs with a longer time coagulation being reentrained into the plume and flowing through the smoke detector computational cell. Predictions were also obtained with a slower coagulation frequency, G = 0.01 ¯s. The predicted time variation of the ratio $C_m(t)$ /$C_N(t)$ is shown in Figure 14. As expected the ratio shows a much

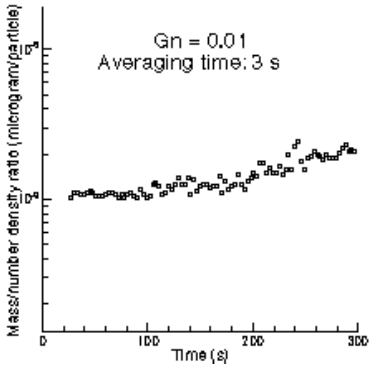

Figure14. Time-averaged (3 s intervals) prediction of the ratio $C_m(t)$ /$C_N(t)$ at the detector location ($G = \Gamma N^o = 0.01$)

gradual rise with time now, indicating that the model simulates the prescribed physics realistically. The differences between the simulations and measurements may be partly experimental uncertainty and partly from the simulation not including a time varying size distribution. A steady state gas burner would be useful in providing a better test of the simulations.

Conclusions

Numerical simulations of smoke transport and smoke coagulation in the fire TF4 (EN54 part 9) were conducted. The simulations were based on the heat release rate as prescribed in the test fire in addition to an estimated smoke yield and initial particle size. The present results provide insights regarding the effect of coagulation on the change in the number concentration and mass per particle in the vicinity of a detector positioned near the ceiling of an enclosure.

Acknowledgements

One of the authors (BF) gratefully acknowledges support from the Building and Fire Research Laboratory at NIST, Gaithersburg, MD where he served as a Guest Researcher during the academic year 1999-00

References

[1] Baum, HR, Rehm RG and Mulholland GW, 'Computations of Fire Induced Flow and Smoke Coagulation' 19th Symposium (International) on Combustion, The Combustion Institute, 1982, p. 921-931

[2] Baum HR, Rehm RG and Mulholland GW, 'Prediction of Heat and Smoke Movement in Enclosure Fires', Fire Safety Journal, 1983, 6, p. 193-201

[3] McGrattan KB., Baum HR. and Rehm RG.,'Large Eddy Simulation of Smoke Movement', Fire Safety Journal, 1998, 30(2), p. 161-178

[4] Baum HR., and McCaffrey BJ., 'Fire Induced Flow Field – Theory and Experiment' Fire Safety Science – Proceedings of the Second International Symposium, 1989, p. 129-148

[5] Jackson MA, and Robins I, 'Gas Sensing for Fire Detection: Measurements of CO, CO2, H2, O2, and Smoke Density in European Standard Fire Tests', 1994, Fire Safety Journal, 22, p. 181-205

[6] Mulholland GW, 'Smoke Production and Properties', NFPA Fire Protection Handbook, Sec. 2, Ch. 15, 1993

[7] Mirme A., Tamm, E. and Siever, U, 'Performance of an Optical and an Ionization Smoke Detector Compared to a Wide Range Aerosol Spectrometer', Internationale Konfernz uber Automatische Brandentdeckung, AUBE 1999, Proceedings, p. 380-391

[8] Ahonen, AI, and Sysio PA, 'A Run-in Test Series of a Smoke Test Room – Tests according to the proposal prEN 54-9', Research Report 139, Technical Research Center of Finland, 1983

[9] Rehm RG. and Baum HR., 'The Equations of Motion of Thermally Driven Buoyant Flows', Journal of Research, National Bureau of Standards, 1978, 83(3), p. 297-308